# Modeling and comparison of superconducting linear actuators for highly dynamic motion

**B.J.H. DE BRUYN, J.W. JANSEN, E.A. LOMONOVA**

*Eindhoven University of Technology*
*Electromechanics and Power Electronics Group*
*Department of Electrical Engineering,*
*PO Box 513, 5600MB, Eindhoven, The Netherlands*
*e-mail: b.j.h.d.bruyn@tue.nl*

**Abstract:** This paper presents a numerical modeling method for AC losses in highly dynamic linear actuators with high temperature superconducting (HTS) tapes. The AC losses and generated force of two actuators, with different placement of the cryostats, are compared. In these actuators, the main loss component in the superconducting tapes are hysteresis losses, which result from both the non-sinusoidal phase currents and movement of the permanent magnets. The modeling method, based on the H-formulation of the magnetic fields, takes into account permanent magnetization and movement of permanent magnets. Calculated losses as function of the peak phase current of both superconducting actuators are compared to those of an equivalent non-cryogenic actuator.

**Key words:** linear motors, loss calculation, high-temperature superconductors, HTS

## 1. Introduction

Linear motors are applied in highly dynamic positioning systems in the semiconductor industry [1]. In photolithographic systems, linear motors move the photomask in a repeated left-to-right sequence to allow scanning exposure of the dies on a wafer. Application of superconducting motors in these systems potentially allows an increase in throughput while lowering the required input power. Losses in the superconducting tapes are a dominant factor in the required cooling power, while the critical current density of the coils wound of superconducting tapes limits the force density that can be achieved.

Various linear actuators exist which incorporate superconducting materials. A linear actuator with a copper stator winding and field-cooled HTS bulk material in the translator was developed for electromagnetic aircraft launch systems [2], where the translator is levitated using HTS bulk levitation components. Another electromagnetic aircraft launch system, with superconducting stator coils and a field-cooled bulk HTS mover, was presented in [3, 4]. The use of trapped field HTS bulks is less suitable for the application described in this paper, since the trapped field attenuates as a result of an applied AC magnetic field [5]. A tubular actuator

with permanent magnet mover and a superconducting stator with a soft magnetic iron core was presented in [6]. For this actuator, loss calculations were presented for sinusoidal excitation of the coils, concluding that the maximum frequency of the coil currents is around 15 Hz in [7].

Hysteresis losses are a major loss component in HTS tapes [8]. Up to now, the evaluation of losses based on a physical model has not been shown for linear actuators. Moreover, it is unknown how the higher harmonics of the phase currents and magnetic flux density applied to superconducting tapes affect the hysteresis losses. For the calculation of losses in superconducting tapes, and stacks of tapes, analytical [9] and numerical methods exist [10]. Numerical methods can include the dependency of the critical current density on the magnetic flux density, and the nonlinear magnetization of structures external to the superconducting tapes. Numerical models are able to include the hysteresis losses as well as the substrate losses in stacks of superconducting coils [11].

The computation time for the hysteresis losses in a finite stack of superconducting tapes can be reduced by representing the stack by a homogeneous bulk element, as is presented for an analytical model in [12]. An equivalent homogenization method is also applied in finite elements models based on the H-formulation of the magnetic field [13] to reduce the number of mesh elements. The homogenization procedure exploits the fact that the current distributions in adjacent tapes are similar, and greatly reduces the required number of mesh elements. This procedure can be applied in the design of superconducting actuators, to evaluate the losses [14].

In this paper permanent magnetization is included in the H-formulation to be able to evaluate the hysteresis losses in highly dynamical superconducting linear actuators with a permanent magnet mover. First, the H-formulation is introduced, and a general model for the superconducting material is given. Then, the two actuator geometries and the required motion profile are presented. Finally, losses as function of the peak phase current are given and for both actuators, and compared to losses in motors with non-cryogenic copper coils.

## 2. Numerical method

Various formulations are suitable for modeling transient behaviour of superconducting tapes [15]. For this work, the H-formulation of the magnetic fields was implemented in COMSOL [16] using zeroth-order edge elements [13]. A particular advantage of this combination of formulation and element type is that the current density derived from the solution is homogeneous within each mesh element. This property simplifies the implementation of a homogeneous bulk model for stacks of superconducting tapes. The H-formulation is obtained by inserting the constitutive relation

$$\mathbf{E} = \rho \, \mathbf{J}, \tag{1}$$

where $\mathbf{E}$, $\rho$ and $\mathbf{J}$ are the electric field strength, resistivity, and current density respectively, in the Maxwell-Faraday equation, which results in

$$-\nabla \times \left(\rho \nabla \times \mathbf{H}\right) = \frac{\partial \mathbf{B}}{\partial t}.$$ (2)

The magnetic flux density $\mathbf{B}$, magnetic field strength $\mathbf{H}$, initial magnetization $\mathbf{M}_0$, relative permeability $\mu_r$, and permeability of free space $\mu_0$ are coupled by the constitutive relation

$$B = \mu_0 \mu_r \mathbf{H} + \mu_0 \mathbf{M}_0.$$ (3)

Assuming $\mu_r = \mu_r \left(|\mathbf{H}|\right)$, the right hand side of (2) is expanded as

$$\frac{\partial B}{\partial t} = \mu_0 \left( \frac{\partial \mu_r \left(|\mathbf{H}|\right)}{\partial t} \mathbf{H} + \mu_r \left(|\mathbf{H}|\right)\frac{\partial \mathbf{H}}{\partial t} + \frac{\partial \mathbf{M}_0}{\partial t} \right).$$ (4)

For a 2D model which is continuous in the *z*-direction, the expanded form of (2) is implemented in COMSOL as

$$\mu_0 = \begin{bmatrix} \dfrac{\partial H_x}{\partial t} \\ \dfrac{\partial H_y}{\partial t} \end{bmatrix} + \nabla \cdot \begin{bmatrix} 0 & E_z \\ -E_z & 0 \end{bmatrix} = -\mu_0 \begin{bmatrix} \dfrac{\partial \mu_r}{\partial t} H_x + \dfrac{\partial M_{0x}}{\partial t} \\ \dfrac{\partial \mu_r}{\partial t} H_y + \dfrac{\partial M_{0y}}{\partial t} \end{bmatrix}.$$ (5)

## 3. Modeling of superconducting material

The superconducting coils in the modeled actuators consist of YBCO tape. The resistivity of superconducting material is described by the macroscopic power law model

$$\rho = \frac{E_c}{J_c} \left| \frac{J}{J_c} \right|^{n-1}.$$ (6)

The threshold voltage, $E_c$, indicates the point of onset of normal conductivity, and the n-value determines the exponent of the $E - J$ curve. The critical current density, $J_c$, is in general dependent on the magnetic flux density perpendicular and parallel to the superconducting tape. This effect is described by the elliptic model

$$J_c = \frac{J_{c0}}{\left( 1 + \dfrac{\sqrt{k^2 |B_{\mathrm{II}}|^2 + |B_{\mathrm{I}}|^2}}{B_0} \right)^\alpha},$$ (7)

which is an extension of the Kim model [17]. The parameters $J_{c0}$, $k$, $B_0$, and α have been obtained by a least square error fit of the elliptic model to Superpower [18] measurement data. The values of all parameters of the modeled superconducting tape are given in Table 1.

It should be noted that these parameters can all vary with the operating temperature. The obtained parameter values are similar to those found in the literature [19] [20].

Table 1. Parameters of the superconducting tape stack

| Parameter name | Symbol | Value |
|---|---|---|
| Spacing between HTS tapes | | 0.293 mm |
| Half-width HTS tape | | 2 mm |
| Thickness HTS layer | | 1 μm |
| Number of turns per coil | | 120 |
| Temperature | | 40 K |
| Critical current density | $J_{c0}$ | 1.49e11 A/m$^2$ |
| Anisotropy factor | $k$ | 0.0786 |
| Field sensitivity parameter | $B_0$ | 0.3365 T |
| Field dependency parameter | $\alpha$ | 0.7 |
| $n$-value | $n$ | 25 |
| Threshold voltage | $E_c$ | 1 μV/m |

In this study, only the losses in the superconducting layer are considered. The instantaneous power loss $P$, in the volume of the superconducting tapes, is calculated as

$$P = \int_{V_{sc}} \mathbf{E} \cdot \mathbf{J} dV,$$ (8)

where $V_{sc}$ is the volume of the superconducting material. In the superconducting actuator model, the stacks of tapes consisting of 120 layers are modeled by 10 homogeneous bulk regions [13].

## 4. Superconducting motor model

The geometries of the two modeled moving-magnet linear motors with superconducting stator coils, geometry A and B, are shown in Figure 1, and the geometric parameters of the actuators are given in Table 2.

The figure shows the lower half of one periodic segment of the total actuators. The actutors consists of a soft magnetic back-iron, superconducting stator coils, and a permanent magnet mover. A periodical boundary is applied at $x = 0$ and $x = 4\tau_p$, while a Dirichlet boundary condition is applied at $y = 0$. It is assumed that the wall thickness of the cryostat $d_{cr}$ is 10 mm. The soft magnetic core, having a saturation flux density of 2.2 T, both reduces the magnetic flux density in the superconducting coils, and increases the magnetic flux density in the air gap, for equal coil current. The teeth of the stator are partially closed to shield the superconucting coils from changes in the magnetic flux density resulting from movement of the peranent magnet translator.

Gometries A and B have different placement of the cryostat around the superconducting coils. In geometry A, individual coils are enclosed in a cryostat, through which the teeth of the core protrude. As a result, the air gap between the stator teeth and the permanent magnets is kept small. A disadvantage of this geometry is the complexity of the cryostat. In geometry B,

the full stator is enclosed by the cryostat. In this case, the air gap depends on the thickness of the cryostat, and is significantly larger than that of geometry A. The cryostat of geometry B, however, is less complex.
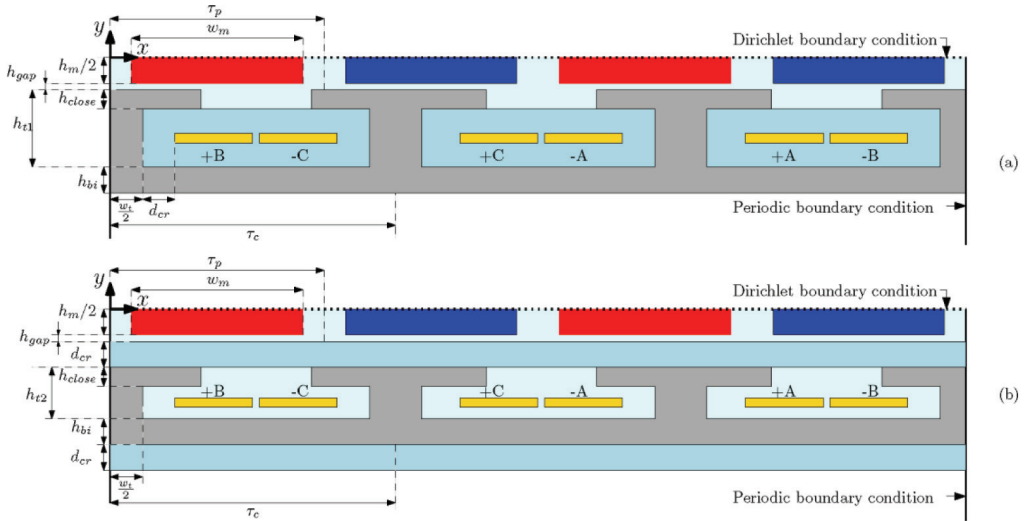


Fig. 1. Geometry of one periodic section of the superconducting actuators with moving magnet translator and superconducting stator coils: (a) geometry A: cryostat around individual coils, (b) geometry B: cryostat around full stator

Table 2. Parameters of the superconducting tape stack

| Parameter name | Symbol | Value |
|---|---|---|
| Actuator depth | | 200 mm |
| Magnetic pole pitch | $\tau_p$ | 100 mm |
| Magnet height | $h_m$ | 20 mm |
| Magnet width | $w_m$ | 40 mm |
| Remanence permanent magnets | $B_{rem}$ | 1.3 T |
| Air gap height | $h_{gap}$ | 1 mm |
| Tooth height geometry A | $h_{t1}$ | 34 mm |
| Tooth height geometry B | $h_{t2}$ | 24 mm |
| Tooth closure height | $h_{close}$ | 10 mm |
| Height of cryostat | $d_{cr}$ | 10 mm |
| Height of superconductor | | 4 mm |
| Height of back-iron | $h_{bi}$ | 15 mm |
| Tooth width | $w_t$ | 30 mm |
| Coil pitch | $\tau_c$ | $(3/4)\,\tau_p$ |

The motor performance is determined for a typical fourth order motion profile of the application, shown in Figure 2.
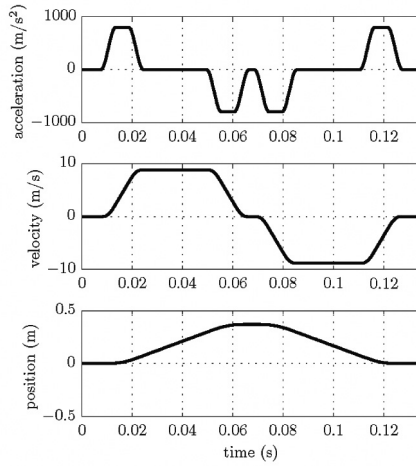
Fig. 2. Fourth order motion profile of the translator

Magnetization of the permanent magnets is included in the finite element models by imposing the time derivative of the magnetization, given by (5), in the region of the permanent magnets. This allows modelling the permanent magnetization and the movement of the permanent magnets without re-meshing the finite element model. The region of the permanent magnet is between $y = 0$ and $y = -h_m/2$. The magnetization is assumed constant in the $y$-direction. Only the time derivative of the initial magnetization $\mathbf{M}_0$ is included in the H-formulation. The magnetization of an individual magnet $\mathbf{M}_n$ having width $W_m$ and center position $x_c$ as function of the $x$-coordinate and time $t$, is described by

$$M_n = \frac{B_{rem}}{\mu_0} \frac{1}{2} \left( \tanh\left( s\left( x - x_c(t) + \frac{W_m}{2} \right) \right) - \tanh\left( s\left( x - x_c(t) - \frac{W_m}{2} \right) \right) \right) \mathbf{e}_y, \tag{9}$$

where $s$ determines the length of the transition region from zero magnetization outside the magnet to the magnetization inside the magnet.
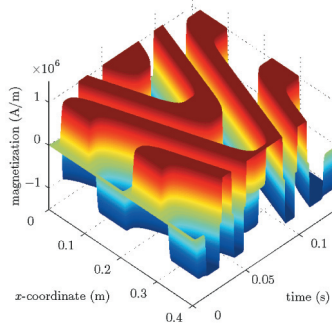


Fig. 3. Magnetization of the magnet region, as function of time and $x$-coordinate

The magnetization of the total magnet array is obtained by a linear combination of (9) with magnets with different center positions and polarities. Since only the time derivative of the magnetization is included, stationary magnets cannot be directly modeled with the given formulation. Therefore, the magnetization of stationary permanent magnets is included in the model by increasing the amplitude of magnetization from zero to the desired value over an interval of time. The *y*-component of the analytically calculated magnetization of the permanent magnet mover is shown in Figure 3. The time derivative of the magnetization function shown there is included as a source term in the finite element model.

The superconducting coils carry a commutated current, which is dependent on the required acceleration, phase angle, phase, and peak current $I_{pk}$. The phase currents, for the given motion profile, for a peak current of 40 A, are shown in Figure 4.
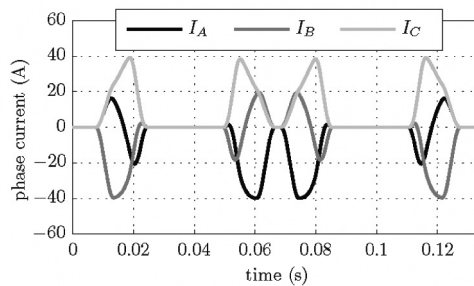


Fig. 4. Superconducting coil phase currents

The losses are calculated for a range of peak currents in the superconducting coils. The zero-field critical current, $I_c$, of one layer of the modeled superconducting tape is equal to 598 A. The peak current density in the superconducting coils is set to a fraction of the single tape field-free critical current density. The motion profile is equal for each calculation, while higher propulsion force is generated for a higher value of peak current. At a higher propulsion force per section, less sections are required for the full actuator.

## 5. Validation of modelling method

The proposed method to include permanent magnetization in the *H*-formulation is validated for the magnetic structure of geometry A. For the validation of the permanent magnet modeling, the superconducting tape regions are modeled as air. The magnetic flux density in the center of the gap between the permanent magnets and the iron core, after initialization of the permanent magnets, is calculated by the transient calculation in the *H*-formulation. The calculated flux density is compared to a magnetostatic calculation of the model in Flux2D [21], which uses the magnetic vector potential formulation. Both models include the nonlinear magnetization of the soft magnetic material. Results of both models are shown in Figure 5.

Some discrepancies are visible where peaks occur in the magnetic flux density, especially in the *x*-direction. These are mainly caused by the finer mesh that is applied in the Flux2D model.

In general, the modeling method of the permanent magnetization in the H-formulation shows good agreement with the results of Flux2D.
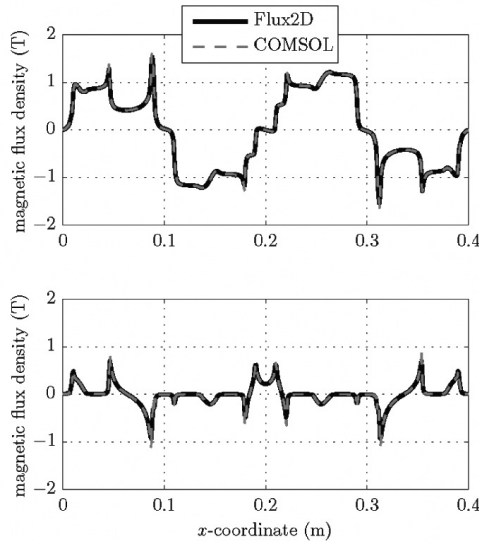


Fig. 5. Comparison of calculated air gap magnetic flux density using transient magnetic simulation with H-formulation in COMSOL and static magnetic simulation in Flux2D. Top: *x*-component of the air gap magnetic flux density. Bottom: *y*-component of the air gap magnetic flux density

# 6. Analysis of results

The nonlinear resistivity of the superconducting tapes leads to an inhomogeneous current distribution in the coils. The current density normalized to the critical current density, in the two coil sides situated in the left slot of geometry A, for a peak coil current of 0.45 $I_c$, at $t = 0.025$ seconds is shown in Figure 6.
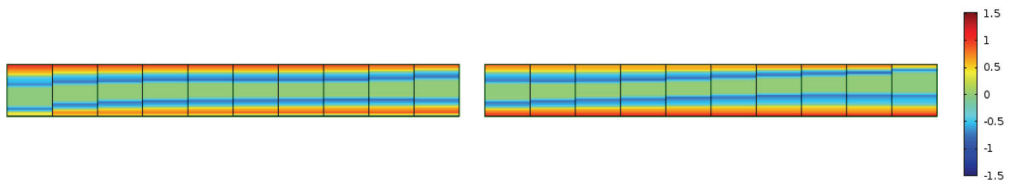


Fig. 6. Current distribution normalized to the critical current density in the coil halves situated in the left slot of geometry A , for peak coil currents of 0.45 $I_c$, at $t = 0.025$ seconds

The ten regions which are used per coil side for the homogenization procedure are visible. The variation of the current density over the coil sides in the horizontal direction is low, which justifies the discretization of 120 layers of tape in 10 regions. This figure shows that the

current density is close to zero in the central part of the superconducting coils, and that at this time instant current is flowing both into as well as out of the plane. Since the power law model is implemented rather than the critical state model, a current higher than the critical current is flowing in some parts of the tape.

The losses resulting from the movement of the permanent magnets and coil currents in the periodic model of both geometry A and B, as function of time and peak current, are shown in Figure 7.
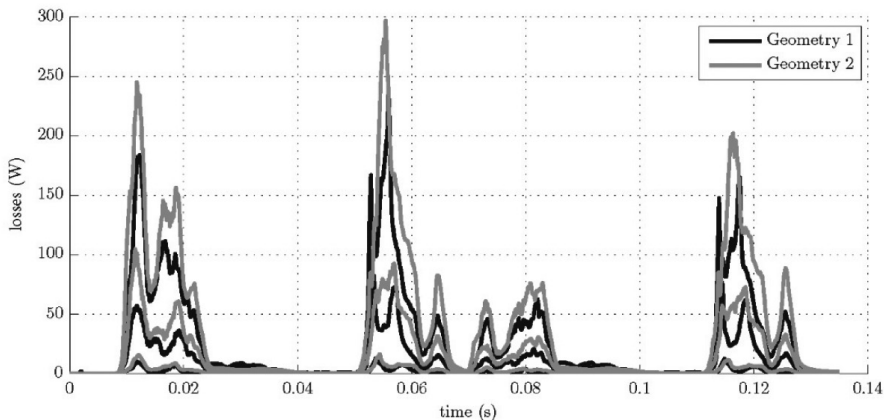


Fig. 7. Losses per periodic section as function of time for peak coil currents
of $0.1 I_c$, $0.2 I_c$, and $0.3 I_c$, for geometries A and B

From this figure it can be concluded that the highly-dynamic motion profile of the superconducting linear actuator does not result in excessive losses for both geometries. Losses occur mainly when a transport current is present in the superconducting coils. Peaks of the losses occur at transients of the superconducting coil transport current. After decrease of the transport current to zero, losses in the superconducting tapes still occur due to movement of the permanent magnets. These losses decrease over time. Currents in the superconducting coils are symmetric around $t = 0.065$, while losses are not, due to the hysteretic behaviour of the superconducting material.

The losses in geometry B are lower than those in geometry A at time intervals where the transport current in the superconducting coils is zero, since at these time instants the losses mainly result from movement of the permanent magnets which are at a larger distance from the coils in geometry B than in geometry A. However, averaged over time the losses in geometry B are 18%, 25%, and 16% higher than in geometry A, for peak coil currents of $0.1 I_c$, $0.2 I_c$, and $0.3 I_c$ respectively. This can be explained by the closer proximity of the iron core to the coils in geometry B compared to geometry A. The closer proximity results in an increase of the magnetic flux density in the superconducting coils, which reduces the critical current density, resulting in higher losses at equal transport currents.

The force as function of time generated by geometry A and B, for peak currents of $0.1 I_c$, $0.2 I_c$, and $0.3 I_c$ are shown in Figure 8.

The force generated by geometry B is significantly lower than the force generated by geometry A, which is a result of the larger air gap in geometry B. At peak currents of 0.1 $I_c$, geometry B generates a peak force 50% higher than geometry A, while at peak currents of 30% of the critical current, geometry B generates a 38% higher force. Both the force ripple resulting from the coil currents, as the cogging force are lower in geometry B than in geometry A.
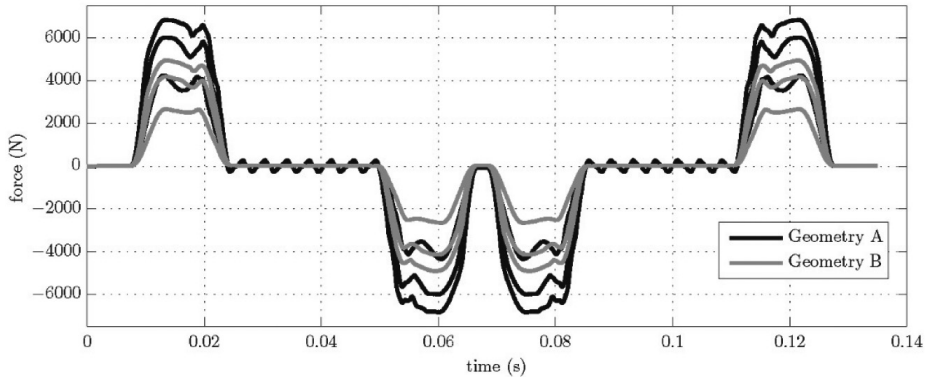


Fig. 8. Force as function of time, generated by geometries A and B at peak coil currents of 0.1 $I_c$, 0.2 $I_c$, and 0.3 $I_c$

To compare the superconducting actuator with geometry A to a conventional actuator, losses are calculated for an equivalent actuator, in which the superconducting coils are replaced by copper coils which fill the full slot area. Losses in the superconducting actuator are compensated by a cryocooler, which achieve approximately 2.5% efficiency for a cold side of 40 K. Therefore, copper losses are compared to the superconductor losses, reflected to room temperature by multiplying them by a factor 40. Time averaged losses as function of peak current for both actuators are shown in Figure 9.
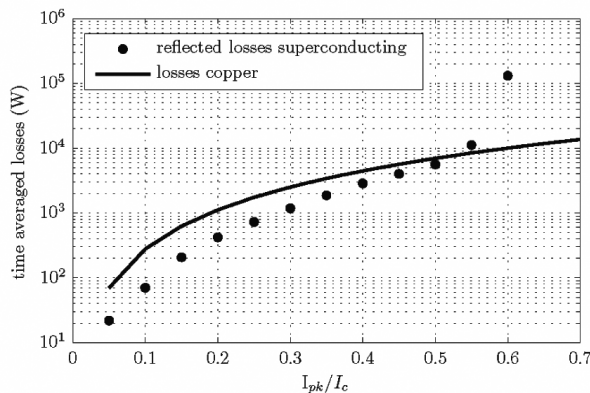


Fig. 9. Time averaged reflected losses of the superconducting actuator with geometry A and losses of the copper coil actuator, as function of the ratio of peak current to zero-field critical current

The figure shows that losses in both conventional and superconducting actuators increase approximately quadratically with the peak current for lower values of the peak phase current. As the peak current reaches the critical current of the coil, losses of the superconducting actuator increase sharply and exceed those of the copper coil actuator. It should be noted that the pole pitch of the superconducting actuator is limited by the minimum bending radius of the superconducting tape, and is not optimal considering force density. For copper coils, this limitation does not exist, such that a higher force can be achieved at a lower dissipation. The force density of superconducting linear actuators is limited by the critical current density and the AC losses that can be cooled by the cryocooler. A rated force of the superconducting actuator can be defined as the rms force at which the AC losses equal the available cooling power. The superconducting actuator cannot be operated at currents above the critical current, while the copper coil actuator can shortly operate at very high currents. Not all loss components occurring in superconducting actuators are included. For example, heat loss through the cryostat, and losses in the current leads can contribute significantly to the total losses.

In the application considered in this paper, a large fraction of the slot area is required for the cryostat. The average current density in the slot is therefore not much higher than can be achieved with conventional copper coils. This disadvantage is smaller for larger scale superconducting machines, such as those used in wind mills, since a lower fraction of the volume of the machine is occupied by the cryostat. In (quasi)DC applications, losses in the superconducting coils are much lower, which allows for a lower operating temperature. In these applications, the average current in the slot can be higher than can be achieved with copper coils.

The evaluation time of the finite element model increases with the value of the peak current density, and varies between 6 and 19 hours on a desktop PC. It should be decreased to be suitable for the design of superconducting linear actuators.

# 7. Conclusions

This paper presented a numerical method for the calculation of hysteresis losses in the superconducting coils of a linear actuator with a permanent magnet mover. The generated force and losses of two actuator concepts were compared. It was found that the actuator in which each coil is enclosed in a separate cryostat obtains lower losses, as well as a higher force, than the actuator in which the stator is fully enclosed in the cryostat. However, the force ripples and cogging force are lowest in the actuator in which the full stator is enclosed in the cryostat. Results show that the average losses resulting from non-sinusoidal commutation of the superconducting coils increases approximately quadratically with peak current at first, then sharply increases above a certain value of peak current. Therefore, over-current operation of superconducting actuators will result in excessive losses, which is a disadvantage compared to non-cryogenic actuators with copper coils. The highly-dynamic motion profile of the superconducting linear actuator does not result in excessive losses for both considered actuator concepts.

## References

 [1] Butler H., *Position Control in Lithographic Equipment [Applications of Control]*. IEEE Control Systems 31(5): 28-47 (2011).
 [2] Jin J.X., Zheng L.H., Guo Y.G. et al., *High-Temperature Superconducting Linear Synchronous Motors Integrated With HTS Magnetic Levitation Components*. IEEE Trans. Applied Superconductivity 22(5): 5202617-5202617 (2012).
 [3] Pina J.M., Neves M.V., Alvarez A., Rodrigues A.L., *Numerical Design Methodology for an All Superconducting Linear Synchronous Motor*. Second IFIP WG 5.5/SOCOLNET Doctoral Conference on Computing, Electrical and Industrial Systems, Costa de Caparica, pp. 553-562 (2011).
 [4] Pina J.M., Martins J., *Control of an electromagnetic aircraft launch system based on a superconducting linear synchronous motor*. Int. Conf. on Compatibility and Power Electronics, pp. 255-259 (2013).
 [5] Jin J., Zheng L., *Trapped Field Attenuation Characteristics of HTS Bulk Magnet Exposed to External Traveling-Wave Magnetic Field in an HTSLSM*. Physics Procedia 36: 866-871 (2012).
 [6] Oswald B., Best K.J., Maier T. et al., *Conceptual design of a SC HTS linear motor*. Superconductor Science and Technology 17(5): S445-S449 (2004).
 [7] Oswald B., Best K.J., Setzer M. et al., *AC Application of HTS Conductors in Highly Dynamic Electric Motors*. J. of Physics: Conference Series 43(1): 800-803 (2006).
 [8] Nguyen D.N., Ashworth S.P., Willis J.O. et al., *A new finite-element method simulation model for computing AC loss in roll assisted biaxially textured substrate YBCO tapes*. Superconductor Science and Technology 23(2): 025001(2010).
 [9] Mikitik G., Mawatari A., Wan A., Sirois F., *Analytical Methods and Formulas for Modeling High Temperature Superconductors*. IEEE Trans. Appl. Supercond. 23(2): 8001920-8001920 (2013).
[10] Grilli F., Pardo E., Stenvall A. et al., *Computation of Losses in HTS Under the Action of Varying Magnetic Fields and Currents*. IEEE Trans. Appl. Supercond. 24(1):78-110 (2014).
[11] Ainslie M.D., Flack T.J., Campbell A.M., *Calculating transport ac losses in stacks of high temperature superconductor coated conductors with magnetic substrates using fem*. Physica C: Superconductivity 472(1): 50-56 (2012).
[12] Prigozhin L., Sokolovsky V., *Computing AC losses in stacks of high-temperature superconducting tapes*. Supercond. Sci. Technol. 24(7): 075012 (2011).
[13] Zermeno V.M.R., Abrahamsen A.B., Mijatovic N. et al., *Calculation of alternating current losses in stacks and coils made of second generation high temperature superconducting tapes for large scale applications*. J. Appl. Phys. 114(17): 173901 (2013).
[14] de Bruyn B.J.H., Jansen J.W., Lomonova E.A., *Superconducting Linear Actuators for Highly Dynamic Motion*. Int. Symposium on Linear Drives for Industry Appl., Aachen (2015).
[15] Lahtinen V., Lyly M., Stenvall A., Tarhasaari T., *Comparison of three eddy current formulations for superconductor hysteresis loss modelling*. Supercond. Sci. Technol. 25(11): 115001 (2012).
[16] *COMSOL 4.3 Multiphysics User's Guide* (2012).
[17] Kim Y.B., Hempstead C.F., Strnad A.R., *Critical Persistent Currents in Hard Superconductors*. Phys. Rev. Lett. 9:306-309 (1962).
[18] www.superpower-inc-com, accessed March (2015).
[19] Souc J., Pardo E., Vojenciak M., Gomory F., *Theoretical and experimental study of AC loss in high temperature superconductor single pancake coils*. Supercond. Sci. Technol. 22(1): 015006 (2009).
[20] Grilli F., Sirois F., Zermeno V., Vojenciak M, *Self-Consistent Modeling of the Ic of HTS Devices: How Accurate do Models Really Need to Be?* IEEE Trans. Appl. Supercond. 24(6): 1-8 (2014).
[21] *Flux2D 11.2.2 User's Guide* (2014).
[22] Tasaki K., Marukawa K., Hanai S. et al., *HTS Magnet for Maglev Applications (1) Coil Characteristics*. IEEE Trans. Appl. Supercond. 16(2): 1100-1103 (2006).
[23] Nemoto K., Terai M., Igarashi M. et al., *HTS Magnet for Maglev Applications (2) Magnet Structure and Performance*. IEEE Trans. Appl. Supercond. 16(2):1104-1107 (2006).